SUPPLEMENTARY INFORMATION

ATP Binding Turns Plant Cryptochrome Into an Efficient Natural Photoswitch

Pavel Müller[1,2*], Jean-Pierre Bouly[2,3,6], Kenichi Hitomi[4], Véronique Balland[5], Elizabeth D. Getzoff[4], Thorsten Ritz[3] & Klaus Brettel[1*]

[1]UMR-8221, CEA-Institut de Biologie et de Technologie de Saclay, CNRS, Université Paris Sud, 91191 Gif-sur-Yvette, France.

[2]UR 5, Physiologie Cellulaire et Moléculaire des Plantes, Université Pierre et Marie Curie, CNRS, 75005 Paris 6, France.

[3]Department of Physics and Astronomy, University of California, Irvine, California 92697, USA.

[4]Department of Integrative Structural and Computational Biology and The Skaggs Institute for Chemical Biology, The Scripps Research Institute, La Jolla, California 92037, USA.

[5]UMR CNRS 7591, Laboratoire d'Electrochimie Moléculaire, Université Paris Diderot, Sorbonne Paris Cité, 75205 Paris 13, France.

[6]Present address: UMR-7238, Génomique des Microorganismes, Université Pierre et Marie Curie, 75006 Paris 6, France.

*e-mail: pavel.muller@cea.fr, klaus.brettel@cea.fr

Supplementary Results

1. ATP Effects in full-length AtCRY1

Before conducting the transient absorption experiments, we have monitored the initial rate of blue-light photoreduction of FAD_{ox} in full-length (wild-type) *At*CRY1 by a highly sensitive fluorescence method (decrease of fluorescence intensity upon conversion of strongly fluorescent FAD_{ox} to weakly fluorescent $FADH^{\bullet}$) in the absence and in the presence of ATP (**Supplementary Fig. 1**). This experiment revealed that ATP does directly enhance the yield of FAD_{ox} photoreduction to $FAD^{\bullet-}/FADH^{\bullet}$ (by a factor of ~3). This effect, however, could in principle originate by several different ways, such as through an increased efficiency of the ET from Trp and Tyr residues to the photoexcited FAD_{ox}, due to decelerated recombination of the formed radical pairs, or by an increased efficiency of $Trp^{\bullet}$/ $TyrO^{\bullet}$ reduction by the extrinsic reductant. With the aim to elucidate the origin of this ATP effect, we have decided to study the system by transient absorption spectroscopy.

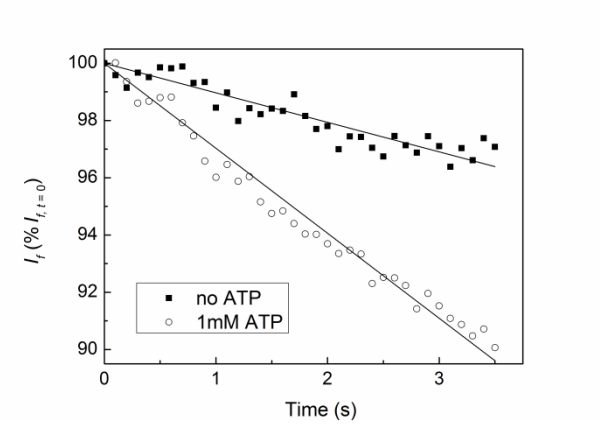

Supplementary Figure 1 | ATP effect on the decay of FAD_{ox} fluorescence in full-length *At*CRY1. Fluorescence was measured at 540 nm under continuous irradiation by the fluorimeter lamp (445 nm) in the absence of ATP (closed squares) and in the presence of 1 mM ATP (open circles) under otherwise identical conditions (50 mM phosphate buffer of pH 7.5, 150 mM NaCl, 12°C). The protein concentration was ~5 μM and β-mercaptoethanol (5 mM) was present as an extrinsic reducing agent.

The experiments presented in the main text were done on truncated *At*CRY1 (*At*CRY1 PHR lacking the flexible C-terminus) because of its convenience for our studies (see main text). Addition of ATP to the full-length *At*CRY1 changed the species kinetics and the absorption spectrum of FAD_{ox} in the same way as in the truncated protein (compare **Supplementary Fig. 2** with **Figs. 2** and **5a** in the main text).

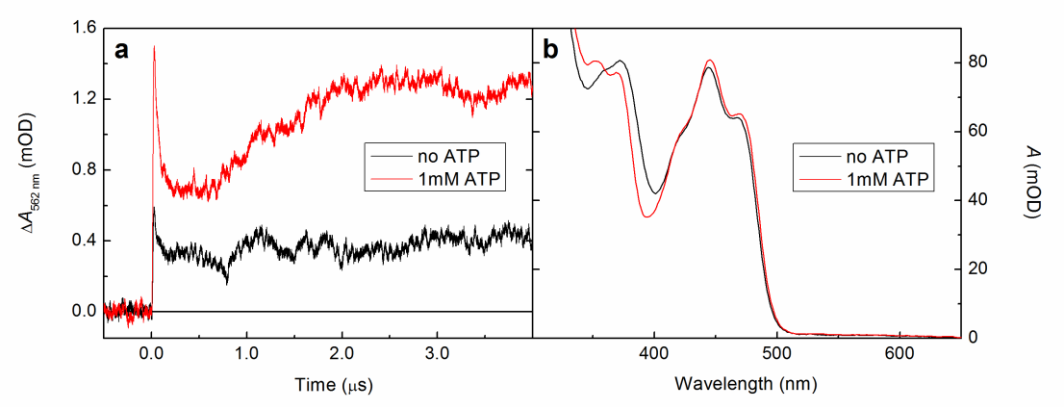

Supplementary Figure 2 | ATP effects on the transient absorption signal and on the stationary FAD_{ox} spectrum in full-length *At*CRY1. (**a**) Kinetic traces recorded at 562 nm upon excitation of FAD_{ox} by a picosecond laser pulse (2.8 mJ at 355 nm, at time zero) in the absence (black) and presence (red) of 1 mM ATP. The poorer signal to noise ratio (compared to the signals in **Figs. 2** and **3** in the main text) is due to a lower protein concentration and lesser signal accumulation. (**b**) Change of FAD_{ox} spectrum upon ATP addition. All samples contained ~7 μM protein, 0.05 M Tris buffer of pH 7.6 and 0.5 M NaCl, and were kept at 1-2°C.

2. Effects of ATP and pH on the stationary absorption spectrum of FAD_{ox}

Decreasing pH results in a similar spectral effect like ATP-binding (**Fig. 5**). **Supplementary Fig. 3b** shows the titration of the pH effect. The change of absorbance at 386 nm (wavelength of maximal change) can be fitted by a titration curve of a monoprotic acid yielding pK_a = 7.38 (± 0.04). This value is in a good agreement with the value obtained from average amplitudes of transient absorption signals from ATP-free samples recorded at 562 nm between 10 and 20 μs (with a major contribution to ΔA from the $FADH^{\bullet}$ – $Trp^{\bullet}$ radical pairs): pK_a = 7.39 (± 0.10) (**Supplementary Fig. 3a**).

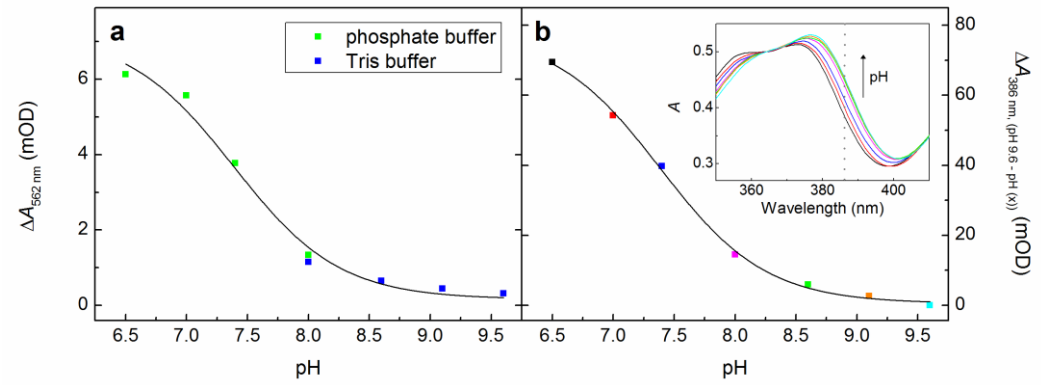

Supplementary Figure 3 | Titration of the pH effects on the $FADH^{\bullet}$ yield and the FAD_{ox} absorption spectrum. (**a**) Average amplitudes of 562 nm transient absorption signals from ATP-free *At*CRY1 PHR samples (45 μM protein) between 10 and 20 μs (with a major contribution to ΔA from the $FADH^{\bullet}$ – $Trp^{\bullet}$ radical pair) plotted against pH. The points were fitted by a titration curve of a monoprotic acid (**Fitting Function 1** with $y = \Delta A_{562\,nm}$, black trace) yielding pK_a = 7.39 (± 0.10). Buffers used: 0.05 M phosphate buffer of pH 6.5 to 8.0 and 0.05 M Tris buffer of pH 8.0 to 9.6, 0.5 M NaCl, 1-2°C, laser energy = 3.5 mJ). (**b**) Absorption differences at the wavelength of maximum change (386 nm) in spectra of ATP-free *At*CRY1 PHR samples (45 μM protein) with respect to the

spectrum recorded at the highest pH (9.6) plotted against pH. The colours of the spectra in the inset correspond to the colours of the points, *i.e.*, to the respective pH. The points were fitted by a titration curve of a monoprotic acid [**Fitting Function 1** with $y(\mathrm{pH}) = A_{386\ \mathrm{nm,\ pH\ 9.6}} - A_{386\ \mathrm{nm,\ pH\ (x)}}$] yielding $\mathrm{p}K_a$ = 7.39 (± 0.10).

Fitting Function 1:

$$y(\mathrm{pH}) = f\frac{1}{1+\frac{10^{-\mathrm{p}K_a}}{10^{-\mathrm{pH}}}} + b$$

y = pH-dependent variable (measured ΔA), f = amplitude scaling factor, b = offset. f, b and $\mathrm{p}K_a$ are fitted to yield a curve with the lowest standard deviation from experimental points described by coordinates [pH;ΔA].

The spectral effect associated with ATP binding to *At*CRY1 (**Fig. 5a**) is similar to that reported for cyclobutane pyrimidine dimer (CPD) lesion to DNA photolyase containing an oxidized FAD cofactor[1,2]. MacFarlane and Stanley[2] reasoned the spectral shift could, in principle, be a result of two possible effects: either a conformational change that modifies orbital interactions between aromatic amino acid residues and the FAD, or an electrochromic shift due to the presence of a dipolar substrate. Based on their study, the authors argue the latter is probably more important. Shifts in the spectrum of the neutral $FADH^{\bullet}$ radical in an *E. coli* PL upon CPD binding were also attributed to the electric dipole of CPD[3]. The ATP-adenine that enters into the pocket in *At*CRY1 (homologous to the CPD binding pocket of photolyase) has a much smaller dipole moment (2.1 – 2.5 D)[4] than two nearly parallel thymines (7.4 ± 0.3 D)[4] of the used CPD[1,2]. Hence the question arises, how can the binding of ATP to *At*CRY1 have an effect on the near UV absorption bands of FAD_{ox} comparable to that of CPD binding to a photolyase (hypsochromic shift in the near UV of approximately the same extent)?

Based on a more-recent crystal structure of an *Anacystis nidulans* CPD photolyase[5] and on our results, we speculate that the observed spectral effects in both PL and *At*CRY1 could be due to a change in the prevailing protonation state and hence change of charge of an amino acid neighbouring the FAD cofactor upon substrate binding. In the CPD photolyase, it could be a glutamic acid (E283 in the *A. nidulans* CPD photolyase) that becomes protonated in the presence of the CPD lesion – due to a stabilization of its protonated form by the formation of hydrogen bonds to the substrate (figure 4D in Ref. [5]). In the case of *At*CRY1, it seems to be D396, the protonated fraction of which increases upon ATP binding, possibly due to ATP-induced conformational changes (see main text for more details), because of replacement of polar solvent molecules in the binding pocket by the less-polar adenine moiety and/or by an electrostatic effect

of the negative charges of the ATP-phosphates. The nature of the binding pocket 'fill' and the negative charges of the phosphates could also have a direct effect on the electronic configuration of FAD_{ox} itself (and thereby on its spectrum). Such an effect may explain why the changes of the *At*CRY1 FAD_{ox} spectrum upon addition of ATP (**Fig. 5a**) and upon decrease of pH (**Fig. 5b**) are, despite their obvious similarity, not completely identical: the band in the visible corresponding to the S0 → S1 (π,π*) transition seems to be more affected by ATP binding than by the pH decrease (that is not expected to change hydrophobicity of the binding pocket).

Addressing the question, whether structural changes induced by ATP binding might be the origin of the spectral changes of FAD_{ox} in *At*CRY1, we compared the two structures by Brautigam *et al.* [6] (with and without an ATP analogue, AMP-PNP): there appears to be no significant change in the conformation of the protein upon binding of the AMP-PNP. Unfortunately, both crystal structures were obtained at pH 5.5, at which D396 should be protonated even in the absence of the ATP analogue. It is hence not clear from these data whether the structure changes when D396(H) loses its proton. Furthermore, the structure lacking AMP-PNP contains a rather non-polar 1,6-hexanediol (crystallization agent) in the binding pocket, which could have similar effects on the pocket conformation like the adenine of ATP/AMP-PNP.

3. Affinity of AtCRY1 to ATP

The analysis of the spectral change as a function of ATP concentration provides a dissociation constant K_d **=** (1.4 ± 0.6) μM for *At*CRY1 PHR (see **Supplementary Fig. 4**). This value can be compared to the published values of 4.2 μM obtained by isothermal titration calorimetry[7] (full-length *At*CRY1, 50 mM Tris buffer of pH 7.4, 0.1M NaCl, 1 mM $MgCl_2$, 0.5 mM DTT, 26°C), or 19.8 μM obtained by liquid scintillation counting[8] (full-length *At*CRY1, 50 mM Tris buffer of pH 7.5, 0.5M NaCl, 10 mM imidazole, 20°C). All these values indicate a very strong affinity assuring that virtually all cryptochrome molecules *in vivo* should bind a molecule of ATP (ATP concentration in plant cells is ≥ 1 mM[9], pH in cytoplasm of higher plant cells is 7.4 – 7.5[10]).

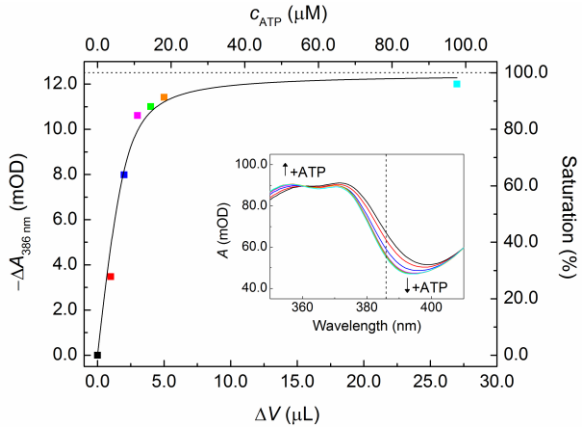

Supplementary Figure 4 | Determination of the dissociation constant of the ATP/*At*CRY1 PHR complex. Absorbance differences at the wavelength of maximum change (386 nm) in spectra (inset) of *At*CRY1 PHR (~8 µM protein, 50 mM phosphate buffer of pH = 7.4, 0.5 M NaCl; initial volume V_0 = 250 µL) upon addition of volumes ΔV of ATP-solution (1 mM, same buffer) with respect to the spectrum recorded at zero concentration of ATP. The spectra, recorded at 10 °C, are corrected for dilution by ATP solution and their colours correspond to the colours of the points, *i.e.*, to their respective ATP concentrations (top) or added ATP volume (bottom). Fitting these points with a protein-ligand saturation isotherm for non-constant protein concentration (black trace, obtained with **Fitting Function 2**) yields a dissociation constant K_d = (1.4 ± 0.6) µM. The dotted line corresponds to 100% saturation (limit of the fitted saturation isotherm) of protein P (CRY) by ligand L (ATP), *i.e.*, 100% of cryptochromes have an ATP bound.

Fitting Function 2:

$$\Delta A_{386} = f\frac{[\mathrm{P}]_0V_0 + [\mathrm{L}]_0\Delta V + K_d(V_0+\Delta V) - \sqrt{\left([\mathrm{P}]_0V_0 + [\mathrm{L}]_0\Delta V + K_d(V_0+\Delta V)\right)^2 - 4[\mathrm{P}]_0[\mathrm{L}]_0V_0\Delta V}}{2[\mathrm{P}]_0V_0}$$

Where ΔA_{386} = dilution-corrected absorbance difference at 386 nm, f = amplitude scaling factor, ΔV = volume of added substrate solution, $[\mathrm{P}]_0$ = initial *At*CRY1 concentration (before substrate addition), V_0 = initial sample volume, $[\mathrm{L}]_0$ = ATP concentration in the stock solution and K_d = dissociation constant. $[\mathrm{L}]_0$, $[\mathrm{P}]_0$ and V_0 are fixed (known) parameters, f and K_d are varied to yield a curve with the lowest standard deviation from experimental points described by coordinates $[\Delta V;\Delta A_{386}]$.

Fitting Function 2 is based on the assumption that ΔA_{386} is proportional to the fractional saturation y:

$\Delta A_{386} = fy$ with $y = \frac{[\mathrm{PL}]}{[\mathrm{P}]+[\mathrm{PL}]}$, where [P] stands for the equilibrium concentration of the free protein (*At*CRY1), [L] for that of the free ligand (ATP) and [PL] for that of the protein–ligand complex.

Replacing [P] and [L] in $K_d = \frac{[\mathrm{P}][\mathrm{L}]}{[\mathrm{PL}]}$ using the expressions for the total concentrations of protein:

$[\mathrm{P}]_{tot} = [\mathrm{P}] + [\mathrm{PL}]$ and ligand $[\mathrm{L}]_{tot} = [\mathrm{L}] + [\mathrm{PL}]$, one obtains

$$[\mathrm{PL}] = \frac{1}{2}\left([\mathrm{P}]_{tot} + [\mathrm{L}]_{tot} + K_d - \sqrt{([\mathrm{P}]_{tot} + [\mathrm{L}]_{tot} + K_d)^2 - 4[\mathrm{P}]_{tot}[\mathrm{L}]_{tot}}\right)$$

and $\Delta A_{386} = f\frac{[\mathrm{PL}]}{[\mathrm{P}]_{tot}} = f\frac{[\mathrm{P}]_{tot}+[\mathrm{L}]_{tot}+K_d-\sqrt{([\mathrm{P}]_{tot}+[\mathrm{L}]_{tot}+K_d)^2-4[\mathrm{P}]_{tot}[\mathrm{L}]_{tot}}}{2[\mathrm{P}]_{tot}}$.

Substituting $[\mathrm{P}]_{tot} = [\mathrm{P}]_0\frac{V_0}{V_0+\Delta V}$ and $[\mathrm{L}]_{tot} = [\mathrm{L}]_0\frac{\Delta V}{V_0+\Delta V}$, one obtains the **Fitting Function 2**.

4. Species kinetics on time scales >1ms

In the absence of an extrinsic reductant, most of the FADH$^\bullet$ – Trp$^\bullet$ radical pairs recombine within a few milliseconds and in about one fifth of all pairs, Trp$^\bullet$ is reduced, presumably by a tyrosine (TyrOH) residue, yielding a longer-lived FADH$^\bullet$ – TyrO$^\bullet$ pair (**Fig. 4** and **Supplementary Fig. 5**). Addition of cysteine can almost completely eliminate the FADH$^\bullet$ – Trp$^\bullet$ recombination and the ET from TyrOH by reducing Trp$^\bullet$, which leads to a high yield of the isolated metastable FADH$^\bullet$ (**Supplementary Fig. 5**). The decay of the curve with the highest cysteine concentration (20 mM; cyan) between t = 0 and t ~ 3ms reflects solely the reduction of the Trp$^\bullet$ radical (which absorbs weakly at 560 nm; see **Fig. 2**) by cysteine, leaving a constant signal due to the absorption of FADH$^\bullet$ (probably with a minor contribution of *ca.* 20% deprotonated semireduced flavin, FAD$^{\bullet-}$; see yields at t = 10 µs in **Supplementary Table 4**).

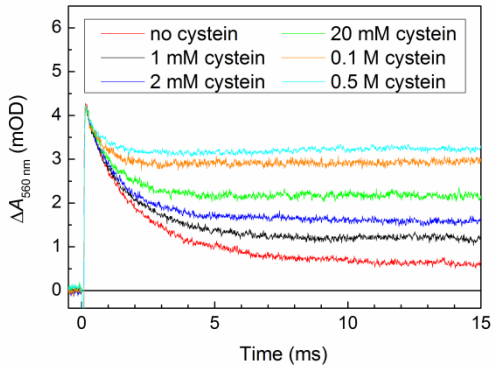

Supplementary Figure 5 | Scavenging of Trp$^\bullet$ radicals by an extrinsic reductant. Millisecond transient absorption kinetics at 560 nm upon excitation of FAD_{ox} by a picosecond laser pulse (2.2 mJ at 355 nm, at time zero) recorded for *At*CRY1 PHR at different concentration of cysteine. Signal amplitudes are corrected for dilution caused by the addition of cysteine solution. The absorbance changes remaining at ~15 ms after excitation reflect isolated metastable FADH$^\bullet$ after reduction of Trp$^\bullet$. The samples contained 35 μM *At*CRY1 PHR, 50 mM phosphate buffer of pH 7.4, 0.5 M NaCl and 1 mM ATP.

The quantum yield of long-lived FADH$^\bullet$ in the presence of 0.5 M cysteine and 1 mM ATP was estimated from the end amplitude in **Supplementary Fig. 5** (3.25 ± 0.05 mOD) with reference to the quantum yield determinations for **Fig. 2** (**Supplementary Information, Section 8**), taking into account the slightly different excitation energies and protein concentrations. Using $\Delta\varepsilon_{560}$(FADH$^\bullet$ – FAD_{ox}) ≐ 3900 $M^{-1}cm^{-1}$ and

$\Delta\varepsilon_{560}(FAD^{\bullet-} - FAD_{ox}) \doteq 450\ M^{-1}cm^{-1}$ and the ratio of $FADH^{\bullet} : FAD^{\bullet-}$ of ~ 4 : 1, we obtain a total $FADH^{\bullet}/FAD^{\bullet-}$ quantum yield of 14 % (± 2%) in the presence of ATP.

Ultimately, $FADH^{\bullet}$ is reoxidized back to FAD_{ox} by molecular oxygen[11], which is a process that is also influenced by ATP[12,13] (time constants of ~2.6 min in the absence *vs.* ~15.3 min in the presence of ATP in air-saturated solutions[12]). The reported slower reoxidation of $FADH^{\bullet}$ to FAD_{ox} in the presence of ATP can be explained by the increase in pK_a of D396(H), as $FADH^{\bullet}$ needs to give off the proton on N5 in order to reoxidize back to FAD_{ox}. The most plausible direct proton acceptor in this reaction is again D396 and, obviously, such PT is possible only if D396 is itself deprotonated. On a time scale of minutes, D396 is probably in protonation equilibrium with the solvent and a much smaller fraction of D396 is unprotonated in the presence of ATP than in its absence.

Surprisingly, on the millisecond timescale in the absence of extrinsic reducing agents, the $FADH^{\bullet} - Trp^{\bullet}$ pairs in the sample containing ATP recombined faster and to a larger extent (relative to their respective initial concentrations) than in the sample lacking ATP (**Fig. 4**). According to the analysis of our data based on the proposed reaction scheme (**Fig. 6**), the presence of ATP strongly increases the ratio of $FADH^{\bullet} - Trp_3^{\bullet}$ to $FADH^{\bullet} - Trp_1^{\bullet}$ pairs by changing the partition between the ultrafast PT pathway and the ET through the tryptophan cascade. Albeit being both composed of the same two chemical species, these radical pairs are qualitatively very different. Not only are the distances between the individual radicals different (which should, everything else equal, favour a faster recombination of $FADH^{\bullet} - Trp_1^{\bullet}$), but also the protonation state of the neighbouring D396 is different in the two cases (prior to proton equilibration with the solvent). While in the $FADH^{\bullet} - Trp_1^{\bullet}$ case, D396 is protonated (it has accepted a proton from $Trp_1H^{\bullet+}$), it is deprotonated in the case of $FADH^{\bullet} - Trp_3^{\bullet}$ since it has protonated $FAD^{\bullet-}$ (and couldn't recover a proton from $Trp_3H^{\bullet+}$ over the large distance). In principle, deprotonated $D396^-$ in the neighbourhood of $FADH^{\bullet}$ allows for an equilibrium $FADH^{\bullet} + D396^- \rightleftharpoons FAD^{\bullet-} + D396(H)$, keeping a certain pool of $FAD^{\bullet-}$ radicals, which might recombine directly with $Trp_3^{\bullet}$ (followed by a protonation of the originating Trp^-: pK_a (TrpH)[14] ~17); *cf.* the corresponding reaction in DNA photolyase[15]. On the other hand, $FADH^{\bullet} - Trp_1^{\bullet}$ cannot recombine but upon two energetically unfavourable back proton transfers: from D396H to $Trp_1^{\bullet}$ and from $FADH^{\bullet}$ to $D396^-$. A comparatively high percentage of $FADH^{\bullet} - Trp_3^{\bullet}$ pairs in the presence of ATP might hence explain the observed faster overall recombination of all $FADH^{\bullet} - Trp^{\bullet}$ pairs.

5. Spectroelectrochemical titration

With the objective to examine whether and to what extent ATP binding influences the redox transitions of the flavin cofactor, we have conducted a spectroelectrochemical titration of *At*CRY1at pH 7.4 with and without 1 mM ATP (see **Supplementary Fig. 6**). We have followed an established procedure, using the same electrochemical cell and the same redox mediators as in our previous study[16]. The only differences were that we used the truncated version of the protein (PHR) instead of the full-length *At*CRY1, 50 mM phosphate buffer instead of 20 mM Tris and 500 mM NaCl instead of 600 mM NaCl. Knowing the total FAD concentration (from the FAD_{ox} spectrum before reduction) and monitoring the change of absorption at 600 nm where the only absorbing species is the semireduced neutral flavin $FADH^{\bullet}$, we could determine the relative amounts of $FADH^{\bullet}$ at the given applied potential. The data in **Supplementary Fig. 6** comprise both oxidative and reductive titrations. The fact that we have not observed any significant hysteresis indicates that the system was close to its thermodynamic equilibrium.

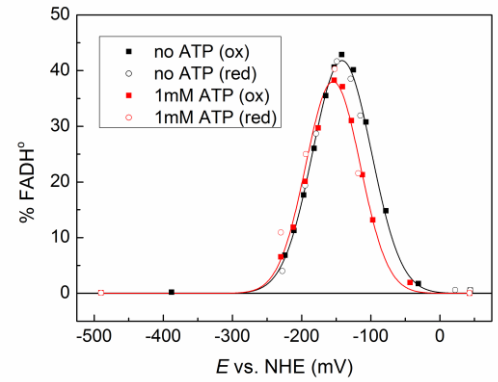

Supplementary Figure 6 | ATP effect on redox titration of *At*CRY1 PHR. Spectroelectrochemical titrations in the absence (black) and in the presence of 1 mM ATP (red) were performed in oxidative (closed squares) and reductive (open circles) directions. The share of neutral semireduced flavin (% $FADH^{\bullet}$) was determined from the absorbance at 600 nm in spectra recorded at the given measured potential *E*. The samples contained ~30 μM protein, 50 mM phosphate buffer of pH 7.4, 0.5 M NaCl, and redox mediators (35 μM each): $Ru(NH_3)_6]Cl_3$, 2-methyl-1,4-naphtoquinone, 2-hydroxy-1,4-naphtoquinone and anthraquinone-2-sulfonate. The samples were kept at 10°C and stirred continuously.

Fitting the experimental data by the two-step Nernst equation with potentials E_1 ($FAD_{ox} \rightarrow FADH^{\bullet}$) and E_2 ($FADH^{\bullet} \rightarrow FADH^{-}$) for the respective redox transitions (see Ref. [16] for more details) yielded E_1 = –129 mV and E_2 = –156 mV (± 16 mV) *vs.* NHE in the absence of ATP, and slightly different E_1 = –146 mV and E_2 = –163 mV (± 20 mV) in the presence of 1 mM ATP. The potential differences of 27 and 17 mV are small (close to the experimental error of ± 20 mV) and can hardly explain the observed strong ATP-effect on *At*CRY1 photochemistry.

6. Construction of the FADH• absorption spectrum

The spectrum of a mixture of FAD_{ox} and FADH• in *At*CRY1 PHR (1 mM ATP, air-saturated solution, spectra normalized to $\varepsilon_{\lambda max,vis}$ (FAD_{ox}) := 11 300 $M^{-1}cm^{-1}$)[17] was recorded 3 min after blue-light photoreduction of *ca.* 25% FAD_{ox} to FADH•. Right after the irradiation, the spectrum was still containing traces of fully reduced $FADH^-$ but three minutes seemed to be sufficient for the faster[11] back reoxidation of $FADH^-$ by molecular O_2 to FAD_{ox} leaving ~15% FADH• (isosbestic points were observed in spectra recorded before irradiation and 3, 5 and 10 min after irradiation but not after 1 min, indicating the presence of a third species ($FADH^-$) immediately after the end of irradiation). The difference spectrum (mixture – FAD_{ox}) multiplied by a factor *f* was then added to the spectrum of pure FAD_{ox}. The value of the factor *f* (~7) was chosen so that the characteristic bands of FAD_{ox} between 400 and 500 nm were no longer apparent in the resulting spectrum of the neutral radical FADH• (**Supplementary Fig. 7**).

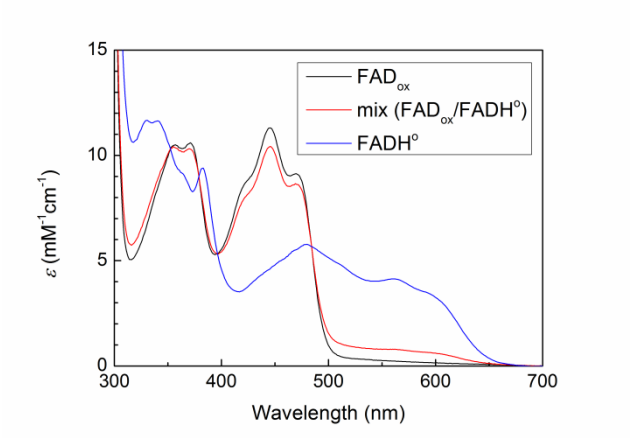

Supplementary Figure 7 | Construction of the FADH• absorption spectrum in *At*CRY1 PHR. The FADH• spectrum was obtained from the spectra of protein containing 100% FAD_{ox} and partially photoreduced protein containing a mixture of FAD_{ox} and FADH• as described above. Spectra were normalized to $\varepsilon_{\lambda max}$($FAD_{ox}$) from the literature[17]: ε_{445}(FAD_{ox}) := 11 300 $M^{-1}cm^{-1}$. The sample containing ~35 µM protein, 50 mM phosphate buffer, 0.5 M NaCl and 1 mM ATP was kept at 10°C.

7. Global analysis of transient absorption kinetics

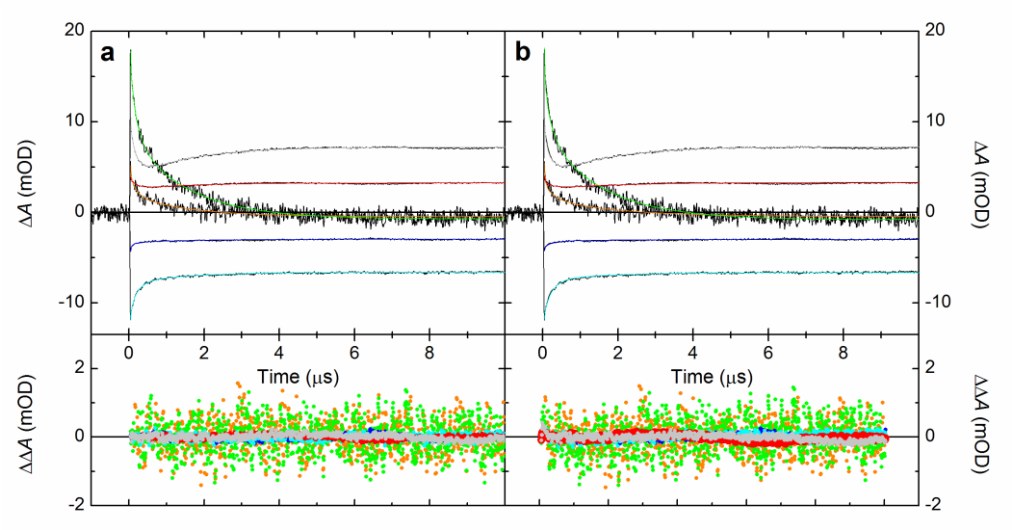

Supplementary Figure 8 | Results of global analysis. (**a**) Best fit obtained using a tri-exponential function (**Fitting Function 3**) with free amplitudes and offsets. The three rate constants (k_1, k_2 and k_3) were shared for all signals, other parameters were free. (**b**) Best fit obtained using a function (**Fitting Function 4**) based on the proposed reaction scheme (**Fig. 6** in the main text). The two lower frames show the residuals of the respective fits **a** and **b**. The values of fixed and fitted parameters are summarized in **Supplementary Tables 1**, **2** and **3**.

Fitting Function 3:

$$\Delta A_{\lambda,\pm}(t) = \Delta A_{1,\lambda,\pm} e^{-k_1 t} + \Delta A_{2,\lambda,\pm} e^{-k_2 t} + \Delta A_{3,\lambda,\pm} e^{-k_3 t} + \Delta A_{0,\lambda,\pm}$$

Supplementary Table 1 | Parameters of the best fit with Fitting Function 3

	−ATP		+ATP	
k_1	4.078×10^7 s^{-1}			
k_2	5.314×10^6 s^{-1}			
k_3	6.599×10^5 s^{-1}			
403 nm	ΔA_1	1.58×10^{-3}	ΔA_1	2.98×10^{-3}
	ΔA_2	1.70×10^{-3}	ΔA_2	6.47×10^{-3}
	ΔA_3	2.36×10^{-3}	ΔA_3	9.09×10^{-3}
	ΔA_0	-0.46×10^{-3}	ΔA_0	-0.73×10^{-3}
457 nm	ΔA_1	-0.74×10^{-3}	ΔA_1	-1.25×10^{-3}
	ΔA_2	-0.22×10^{-3}	ΔA_2	-2.86×10^{-3}
	ΔA_3	-0.37×10^{-3}	ΔA_3	-1.19×10^{-3}
	ΔA_0	-2.97×10^{-3}	ΔA_0	-6.60×10^{-3}
562 nm	ΔA_1	0.33×10^{-3}	ΔA_1	1.74×10^{-3}
	ΔA_2	1.07×10^{-3}	ΔA_2	4.93×10^{-3}
	ΔA_3	-0.72×10^{-3}	ΔA_3	-3.43×10^{-3}
	ΔA_0	3.25×10^{-3}	ΔA_0	7.19×10^{-3}

Fitting Function 4:

$$\Delta A_{\lambda,\pm}(t) = \Delta A'_{\lambda,\pm} e^{-k'_1 t} + \left[c_{\alpha,\pm} \left\{ \Delta\varepsilon_{A,\lambda} e^{-(k'_{2,\pm} - k_{AC',\pm})t} + \Delta\varepsilon_{B,\lambda} \left(\frac{-k_{AB,\pm}}{k'_{2,\pm} - k_{AC',\pm}} e^{-(k'_{2,\pm} - k_{AC',\pm})t} + \frac{k_{AB,\pm}}{k'_{2,\pm} - k_{AC',\pm}} \right) \right\} + \right.$$

$$c_{\beta,\pm} \left\{ \Delta\varepsilon_{A,\lambda} e^{-k'_{2,\pm} t} + \Delta\varepsilon_{B,\lambda} \left(\frac{-k_{AB,\pm}(k'_{2,\pm} - k'_{3,\pm} + k_{BC,\pm})}{k'_{2,\pm}(k'_{2,\pm} - k'_{3,\pm})} e^{-k'_{2,\pm} t} + \frac{k_{AB,\pm} k_{BC,\pm}}{k'_{3,\pm}(k'_{2,\pm} - k'_{3,\pm})} e^{-k'_{3,\pm} t} + \frac{k_{AB,\pm}(k'_{3,\pm} - k_{BC,\pm})}{k'_{2,\pm} k'_{3,\pm}} \right) + \right.$$

$$\left. \left. \Delta\varepsilon_{C,\lambda} \left(\left(\frac{k_{AB,\pm} k_{BC,\pm}}{k'_{2,\pm}(k'_{2,\pm} - k'_{3,\pm})} - \frac{k_{AC',\pm}}{k'_{2,\pm}} \right) e^{-k'_{2,\pm} t} - \frac{k_{AB,\pm} k_{BC,\pm}}{k'_{3,\pm}(k'_{2,\pm} - k'_{3,\pm})} e^{-k'_{3,\pm} t} + \frac{k_{AB,\pm} k_{BC,\pm}}{k'_{2,\pm} k'_{3,\pm}} + \frac{k_{AC',\pm}}{k'_{2,\pm}} \right) \right\} + c_{\gamma,\pm} \Delta\varepsilon_{C,\lambda} \right] d$$

Supplementary Table 2 | Extinction coefficients of transient species from the best fit with Fitting Function 4

		$\Delta\varepsilon/\varepsilon$ [M^{-1}cm^{-1}]		
species	**λ (nm)**	**initial value**	**tolerance interval**	**fit value**
FADH$^{\bullet}$ – FAD$_{ox}$	403	−2250	± 750	−2658
	457	−4500	± 0	
	562	3900	± 0	
FAD$^{\bullet-}$ – FAD$_{ox}$ [18]	403	6000	± 1000	6699 *
	457	−4800	± 800	−5359 *
	562	400	± 70	446 *
TrpH$^{\bullet+}$ [19]	403	650	± 0	
	457	450	± 0	
	562	3000	± 0	
Trp$^{\bullet}$ [19]	403	200	± 0	
	457	1000	± 0	
	562	850	± 0	

* The ratio of the $\Delta\varepsilon$ values at 403, 457 and 562 nm was fixed to 15 : -12 : 1 (from the difference spectrum in ref [18], see Methods).

Supplementary Table 3 | Concentrations and rate constants of the best fit with Fitting Function 4

−ATP			**+ATP**		
$\Sigma(c_\alpha + c_\beta + c_\gamma)$	8.71 × 10^{-7} M		$\Sigma(c_\alpha + c_\beta + c_\gamma)$	25.23 × 10^{-7} M	
c_α	0.58 × 10^{-7} M	(6.7%)	c_α	0.00 × 10^{-7} M	(0.0%)
c_β	5.15 × 10^{-7} M	(59.1%)	c_β	21.89 × 10^{-7} M	(86.8%)
c_γ	2.98 × 10^{-7} M	(34.2%)	c_γ	3.34 × 10^{-7} M	(13.2%)
k_1'	4.08 × 10^{7} s^{-1}	(*fixed*)*	k_1'	4.08 × 10^{7} s^{-1}	(*fixed*)**
k_2'	4.02 × 10^{6} s^{-1}		k_2'	4.79 × 10^{6} s^{-1}	
k_3'	5.38 × 10^{5} s^{-1}		k_3'	6.48 × 10^{5} s^{-1}	
k_{AB}	2.41 × 10^{6} s^{-1}		k_{AB}	2.84 × 10^{6} s^{-1}	
$k_{AC'}$	1.22 × 10^{6} s^{-1}		$k_{AC'}$	0.38 × 10^{6} s^{-1}	
k_{AD}	0.39 × 10^{6} s^{-1}		k_{AD}	1.57 × 10^{6} s^{-1}	
k_{BC}	3.39 × 10^{5} s^{-1}		k_{BC}	4.54 × 10^{5} s^{-1}	
k_{CB}	1.99 × 10^{5} s^{-1}		k_{CB}	1.94 × 10^{5} s^{-1}	

** this rate constant reflects the instrument response to absorption changes that are too fast to be resolved correctly under the given experimental conditions. It was fixed at the value obtained in the best fit with **Fitting Function 3**.

Supplementary Chart 1 | Notations, simplified reaction schemes and equations used to derive Fitting Function 4

D396⁻ at time of excitation	**D396(H)** at time of excitation	
Pathway α	Pathway β	Pathway γ
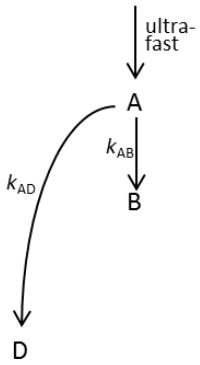	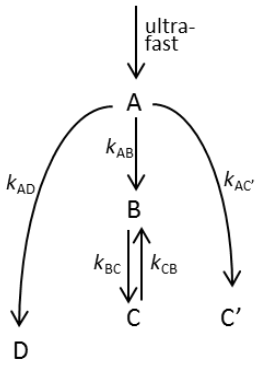	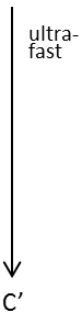
$\frac{dc_A(t)}{dt} = -(k_{AB}+k_{AD})c_A(t)$	$\frac{dc_A(t)}{dt} = -(k_{AB}+k_{AC'}+k_{AD})c_A(t)$	
$\frac{dc_B(t)}{dt} = k_{AB}c_A(t)$	$\frac{dc_B(t)}{dt} = k_{AB}c_A(t) - k_{BC}c_B(t) + k_{CB}c_C(t)$	
$\frac{dc_D(t)}{dt} = k_{AD}c_A(t)$	$\frac{dc_C(t)}{dt} = k_{BC}c_B(t) - k_{CB}c_C(t)$	
	$\frac{dc_{C'}(t)}{dt} = k_{AC'}c_A(t)$	
	$\frac{dc_D(t)}{dt} = k_{AD}c_A(t)$	
$c_A(0) = c_\alpha$	$c_A(0) = c_\beta$	$c_A(0) = c_B(0) = c_C(0) = 0$
$c_B(0) = c_C(0) = c_{C'}(0) = 0$	$c_B(0) = c_C(0) = c_{C'}(0) = 0$	$c_{C'}(0) = c_\gamma$
$c_D(0) = c_D^{t<0} - c_\alpha$	$c_D(0) = c_D^{t<0} - c_\beta$	$c_D(0) = c_D^{t<0} - c_\gamma$
$c_A(t) = c_\alpha e^{-(k_2'-k_{AC'})t}$	$c_A(t) = c_\beta e^{-k_2't}$	$c_A(t) = 0$
$c_B(t) = c_\alpha \frac{k_{AB}}{k_2'-k_{AC}}\left(1-e^{-(k_2'-k_{AC'})t}\right)$	$c_B(t) = c_\beta\left(-\frac{k_{AB}(k_2'-k_3'+k_{BC})}{k_2'(k_2'-k_3')}e^{-k_2't} + \frac{k_{AB}k_{BC}}{k_3'(k_2'-k_3')}e^{-k_3't} + \frac{k_{AB}(k_3'-k_{BC})}{k_2'k_3'}\right)$	$c_B(t) = 0$
$c_C(t) = 0$	$c_C(t) = c_\beta\left(\frac{k_{AB}k_{BC}}{k_2'(k_2'-k_3')}e^{-k_2't} - \frac{k_{AB}k_{BC}}{k_3'(k_2'-k_3')}e^{-k_3't} + \frac{k_{AB}k_{BC}}{k_2'k_3'}\right)$	$c_C(t) = 0$
$c_{C'}(t) = 0$	$c_{C'}(t) = c_\beta\frac{k_{AC'}}{k_2'}\left(1-e^{-k_2't}\right)$	$c_{C'}(t) = c_\gamma$
$c_D(t) = c_D^{t<0} - c_A(t) - c_B(t)$	$c_D(t) = c_D^{t<0} - c_A(t) - c_B(t) - c_C(t) - c_{C'}(t)$	$c_D(t) = c_D^{t<0} - c_\gamma$

Calculating for each fraction $\Delta A_\lambda(t) = \sum_i A_{i,\lambda}(t) - A_\lambda^{t<0}$ with $A_{i,\lambda}(t) = \varepsilon_{i,\lambda}\, c_i(t) d$ and $A_\lambda^{t<0} = \varepsilon_{D,\lambda} c_D^{t<0} d$ and summing the contributions from the three pathways, allowing the initial concentrations c_α, c_β and c_γ and all rate constants to be different in the presence (index +) and absence (-) of ATP and adding a term $\Delta A'_{\lambda,\pm} e^{-k_1't}$ that accounts for instrument limited fast absorption changes, one obtains Fitting Function 4.

Notations

A = $FAD^{\bullet-} - Trp_3H^{\bullet+}$; **B** = $FAD^{\bullet-} - Trp_3^{\bullet}$; **C** = $FADH^{\bullet} - Trp_3^{\bullet}$; **C'** = $FADH^{\bullet} - Trp_1^{\bullet}$; **D** = $FAD_{ox} - TrpH$. $k_2' = k_{AB} + k_{AC'} + k_{AD}$; $k_3' = k_{BC} + k_{CB}$.

$c_i(t)$: Concentration of species i at time t. $c_D^{t<0}$: Concentration of D before excitation. c_α, c_β, c_γ: Concentrations using pathways α, β, γ, resp.

$A_{i,\lambda}(t)$: Absorbance at wavelength λ due to species i at time t. $\varepsilon_{i,\lambda}$: Molar decadic absorption coefficient of species i at wavelength λ.

d: Optical path length. $\Delta A_\lambda(t)$: Absorption change at wavelenth λ at time t. $\Delta\varepsilon_{i,\lambda} = \varepsilon_{i,\lambda} - \varepsilon_{D,\lambda}$ $\Delta\varepsilon_{C',\lambda} = \Delta\varepsilon_{C,\lambda}$

8. Radical pair quantum yields

At the same geometry and excitation energy (at 355 nm) as in **Fig. 2**, 44.7 µM $[Ru(bpy)_3]Cl_2$ solution yielded an averaged absorption change of 6.49 mOD at 562 nm. Using ε_{355} = 5865 $M^{-1}cm^{-1}$ for the ground state of $[Ru(bpy)_3]Cl_2$ and $\Delta\varepsilon_{562}$ = 913 $M^{-1}cm^{-1}$ for the transition to its long-lived excited state, we obtain a fluence of ~7.5×10^{15} photons per cm^2 per one excitation pulse. This fluence is expected to excite c_{exc} = 12.7 µM FAD_{ox} in the *At*CRY1samples used in **Fig. 2** (47µM protein, ε_{355} = 10450 $M^{-1}cm^{-1}$ for FAD_{ox}). The quantum yield $\Phi_i(t)$ of species *i* at time *t* was calculated from $\Phi_i(t) = c_i(t)/c_{exc}$, where $c_i(t)$ is the concentration of species *i* at time *t* obtained from the model-based fit of the experimental data.

Supplementary Table 4|Quantum yields of transient radical pairs*

	$\Phi(t = 0)$**		$\Phi(t = 10\ \mu s)$	
	-ATP	**+ATP**	**-ATP**	**+ATP**
$FAD^{\bullet-}$ – $Trp_3H^{\bullet+}$	4.5 %	17.3 %	0.0 %	0.0 %
$FADH^{\bullet}$ – $Trp_1^{\bullet}$	2.4 %	2.6 %	3.6 %	4.0 %
$FADH^{\bullet}$ – $Trp_3^{\bullet}$	0.0 %	0.0 %	1.5 %	7.2 %
$FAD^{\bullet-}$ – $Trp_3^{\bullet}$	0.0 %	0.0 %	1.3 %	3.1 %
Σ	**6.9 %**	**19.9 %**	**6.4 %**	**14.3 %**

* at pH 7.4; calculated using equations in **Supplementary Chart 1** and the best fit parameters from **Supplementary Table 3**
** reactions preceding formation of $FAD^{\bullet-}$ – $Trp_3H^{\bullet+}$ and of $FADH^{\bullet}$ – $Trp_1^{\bullet}$ were not considered

In a previous study[20], performed in the absence of ATP on full-length *At*CRY1 at 12°C, we have reported a quantum yield of only ~2% for the $FADH^{\bullet}$ – $Trp^{\bullet}$ pairs, *i.e.*, approximately 2.5 times lower than the present estimate (at late times) in the truncated protein at 0-2°C. The deviation is most likely mainly due to a difference in pH. In fact, in our previous study, the pH of the Tris buffer (7.5) was determined at 25°C and its rather strong temperature dependence[21] was ignored. We estimate the real pH under the experimental conditions of our previous study (12 °C) was ~7.85. From our present titration of the signal amplitude in the absence of ATP (**Supplementary Fig. 3a**), one obtains a quantum yield of ~2.5% for the $FADH^{\bullet}$ – $Trp^{\bullet}$ pairs at pH 7.85. The remaining deviation may be due to an insufficient time-resolution (~100 µs) in the previous study and to the difference in temperature (that may also have affected protein stability).

SUPPLEMENTARY REFERENCES

1. Jorns, M. S., Wang, B., Jordan, S. P. & Chanderkar, L. P. Chromophore function and interaction in *Escherichia coli* DNA photolyase: reconstitution of the apoenzyme with pterin and/or flavin derivatives. *Biochemistry* **29**, 552–61 (1990).
2. MacFarlane, A. W. & Stanley, R. J. Evidence of powerful substrate electric fields in DNA photolyase: implications for thymidine dimer repair. *Biochemistry* **40**, 15203–14 (2001).
3. Murphy, A. K, Tammaro, M., Cortazar, F., Gindt, Y. M. & Schelvis J. P. M. Effect of the cyclobutane cytidine dimer on the properties of *Escherichia coli* DNA photolyase. *J. Phys. Chem. B* **112**, 15217–26 (2008).
4. Berezhnoy, A. Y. & Duplij, S. A. Dependence of nucleotide physical properties on their placement in codons and determinative degree *J. Zhejiang. Univ. SCI.* **6B(10)**, 948–60 (2005).
5. Mees, A. *et al.* Crystal structure of a photolyase bound to a CPD-like DNA lesion after in situ repair. *Science* **306** (5702), 1789–93 (2004).
6. Brautigam, C. A. *et al.* Structure of the photolyase-like domain of cryptochrome 1 from *Arabidopsis thaliana*. *Proc. Natl. Acad. Sci. U.S.A.* **101**, 12142–47 (2004).
7. Ozgür, S. & Sancar, A. Analysis of autophosphorylating kinase activities of *Arabidopsis* and human cryptochromes. *Biochemistry* **45**, 13369–74 (2006).
8. Bouly, J. P. *et al.* Novel ATP-binding and autophosphorylation activity associated with *Arabidopsis* and human cryptochrome-1. *Eur. J. Biochem.* **270**, 2921–28 (2003).
9. Blatt, M. R. Electrical characteristics of stomatal guard cells: the contribution of ATP-dependent, "electrogenic" transport revealed by current-voltage and difference-current-voltage analysis. *J. Membrane Biol.* **98**, 257–74 (1987).
10. Shen, J. *et al.* Organelle pH in the *Arabidopsis* endomembrane system. *Mol. Plant* **6**, 1419–37 (2013).
11. Müller, P. & Ahmad, M. Light-activated cryptochrome reacts with molecular oxygen to form a flavin-superoxide radical pair consistent with magnetoreception. *J. Biol. Chem.* **286**, 21033–40 (2011).
12. Burney, S. *et al.* Conformational change induced by ATP binding correlates with enhanced biological function of *Arabidopsis* cryptochrome. *FEBS Letters* **583**, 1427–33 (2009).
13. Immeln, D., Schlesinger, R., Heberle, J. & Kottke, T. Blue light induces radical formation and autophosphorylation in the light-sensitive domain of *Chlamydomonas* cryptochrome. *J. Biol. Chem.* **282**, 21720–28 (2007).
14. Yagil, G. The proton dissociation constant of pyrrole, indole and related compounds. *Tetrahedron* **23**, 2855–61 (1967).
15. Byrdin, M. *et al.* Intraprotein electron transfer and proton dynamics during photoactivation of DNA photolyase from *E. coli*: review and new insights from an ''inverse'' deuterium isotope effect. *Biochim. Biophys. Acta* **1655**, 64–70 (2004).
16. Balland, V. Byrdin, M., Eker, A. P. M., Ahmad, M. & Brettel, K. What makes the difference between a cryptochrome and DNA photolyase? A spectroelectrochemical comparison of the flavin redox transitions. *J. Am. Chem. Soc.* **131**, 426–27 (2009).
17. Macheroux, P. UV-visible spectroscopy as a tool to study flavoproteins. In Chapman, S.K. & Reid, G.A. *Flavoprotein protocols.* **131**, 1–7 (Humana Press, Totowa, N.J., 1999).
18. Berndt, A. *et al.* A novel photoreaction mechanism for the circadian blue light photoreceptor *Drosophila* cryptochrome. *J. Biol. Chem.* **282**, 13011–21 (2007).
19. Solar, S., Getoff, N., Surdhar, P. S., Armstrong, D. A. & Singh, A. Oxidation of tryptophan an *N*-methylindole by N_3, Br_2^-, and $(SCN)_2^-$ radicals in light- and heavy-water Solutions: a pulse radiolysis study. *J. Phys. Chem.* **95**, 3639–43 (1991).
20. Giovani, B., Byrdin, M., Ahmad, M. & Brettel, K. Light-induced electron transfer in a cryptochrome blue-light photoreceptor. *Nature Struct. Biol.* **10**, 489–90 (2003).
21. Durst, R. A. & Staples, B. R. Tris/Tris·HCl: A standard buffer for use in the physiological pH range. *Clin. Chem.* **18**, 206–08 (1972).